Analysis of the Force Ripples of a Current Loaded PMLSM

Ghislain Remy, Julien Gomand, Abdelmounaïm Tounzi*, Pierre-Jean Barre

Ecole Nationale Supérieure d'Arts et Métiers, Lille, France
Laboratoire d'Electrotechnique et d'Electronique de Puissance de Lille (L2EP)
Tel: (33)320.622.246, fax: (33)320.622.759, e-mail: barre@lille.ensam.fr

* Université des Sciences et Techniques de Lille, France
Laboratoire d'Electrotechnique et d'Electronique de Puissance de Lille (L2EP)

***Abstract* – This paper presents an analysis of the force ripples of an open slot permanent magnet linear synchronous motor (PMLSM). In addition to the no-load case, we study the influence of the current magnitude on these forces. First, the studied PMSLM and its main features are introduced. Then, we present the 2D-FEM model used to study the motor. The methods used to calculate the force and the meshing procedures are also highlighted. The calculated no-load force is compared to measurements. Lastly, the validated model is used to study the influence of the current magnitude on the force ripples at load.**

I. INTRODUCTION

Surface Permanent Magnet Synchronous Machines (PMLSM) are widely used in the industrial framework [1], [2]. These structures allow the achievement of very high performances (power to weight ratio, high dynamics) and are relatively easy to control. These performances have been increased, in the last few years, by using rare-earth permanent magnets, which have very high residual magnetic flux densities [3]. However, the use of such permanent magnets induces some modifications on the operating of the PMSM. Indeed, due to the significant value of their magnetic characteristics, the needed PM thickness is very low, which leads to a thin equivalent air-gap. Therefore, the yoke is very burdened magnetically, so we have to consider both the variation of the armature inductances [4] and the force ripples which then depend on the permanent magnet position and the current magnitude.

The positioning performances of a PMLSM control mainly depend on the accuracy of the lumped parameters of the used analytical model. Besides, the identification of unwelcome perturbations such as the force ripples is also very important. Compared to resistance or inductance parameters, the case of the force ripples is somewhat complicated. Currently, in the control scheme, force ripple compensation only concerns the detent forces, whatever the operating conditions of the system. However, these detent forces are only defined as force ripples at no-load, *i.e.* with no-current.

Force ripples at load are modified by the supplied currents. Thus, without an adapted control, these oscillations become problematic in contouring applications. Therefore, a surface map of the force ripples is required as a function of both the current magnitude and the moving part position with regard to the PMs. As an accurate experimental identification of such a lookup-table is fastidious, numerical modelling is an efficient solution.

In this paper, the aim is to study the influence of the supplied currents on the force ripples in an open-slotted PMLSM. It can be considered as an excited variable reluctance machine with an optimized ratio between teeth and magnets size, which normally avoids force ripples [5]. Therefore, it is unsuitable to skew either the teeth or the magnets to avoid force ripples without highly reducing the force to volume ratio.

In a first part, we present the studied PMSLM with an open slotted primary and give its specifications.

The second part is devoted to the 2D-FEM used to study the structure. The meshing procedures and the force calculation method are introduced. The aim is to obtain accurate force results taking into account the non-linear ferromagnetic saturation. Then, the FEM calculation principle is validated, thanks to an experimental estimation of the force ripples.

In the last part, the influence of the current magnitude on the force ripples is investigated. Predominant frequencies of the force ripples will be studied and discussed.

II. DESCRIPTION OF THE STUDIED PMLSM

The studied system is a LMD10-050 linear motor from the ETEL Company, used in many high precision, high speed positioning applications, such as Pick-and-Place systems in the semiconductor industry. Figure 1 shows a picture of the studied machine and Table 1 summarizes its main features.

With a classical PMLSM control (cascaded closed loops with IP controllers only), such linear motor could reach a positioning accuracy of less than 10µm.

Fig.1. Flat Ironcore PMLSM, LMD10-050 (ETEL).

TABLE I
SPECIFICATIONS OF THE LMD10-050 [6]

Rated Current	Maximal Current	Detent Force	Rated Force	Maximal Force
2Arms	7.9Arms	5N	130N	554N

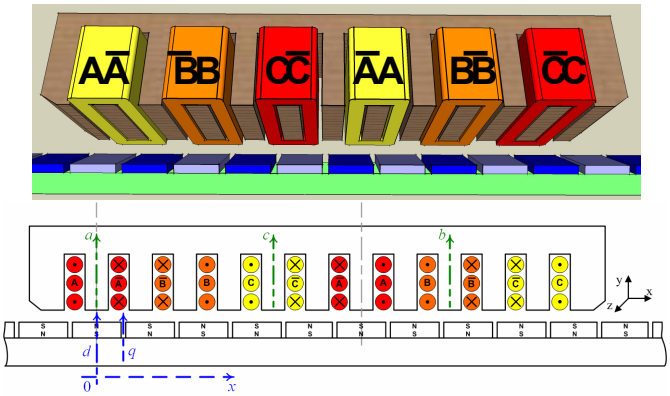

Fig. 2a. 3D view of a section of the whole PMLSM
2b. 2D cutting view of the studied PMLSM [1].

This actuator consists of two main parts:

- The primary part, which is the mobile one. It is teethed and includes the three-phase concentrated windings.
- The secondary part, which is fixed and composed of a set of alternating Nd-Fe-B magnets stuck on the surface of a massive ferromagnetic material.

Figures 2a and 2b respectively give a 3D view of the winding arrangement and a 2D cutting view of the structure.

This kind of open slot PM synchronous structure, which has recently been the subject of greater interest, is in fact a variable reluctance machine excited by PM. Let N_s denote the stator tooth number, p_a the armature pole pairs constituted by concentrated windings and p_m the alternated pairs of magnets. When the armature windings are supplied by a balanced current system of angular frequency ω, the electromagnetic conversion is achieved via the interaction of both fields through the reluctance of the stator teeth. To obtain a continuous conversion of the energy, the following relation:

$$N_s = \pm k(p_a \pm p_m) \tag{1}$$

which links the teeth to the polarity numbers has to be respected. Thus, the structure operates in a manner similar to that of a smooth rotor synchronous machine, with the following synchronous speed in the rotary case:

$$\Omega = \frac{\omega}{kp_m} \tag{2}$$

Then, this motor can theoretically be considered as a non-salient pole machine: its structure has no saliency which could infer inductance variations. Furthermore, the magnet pole pitch τ_p is smaller than the tooth pitch of the stator and the ratio between both pole pitches is designed so that the induced electromotive forces are sinusoidal functions of the inductor position. Besides, this ratio is also chosen to minimize the detent force magnitude, *i.e.* force ripples at no-load.

Even if this structure can be considered as a smooth rotor synchronous machine, its operating remains dependent on the interaction between both PM and armature magnetomotive force (mmf) through the air gap reluctance. Therefore, it is unsuitable to skew either the teeth or the magnets to avoid the residual force ripples.

In the case of the studied PMSLM, N_s=12, p_a=1, p_m=5 and k=2.

III FEM CALCULATION METHODOLOGY

The electromagnetic forces in electrical systems can be calculated by different methods [7]. However, in most of the FEM codes, two approaches are generally used:

- The Virtual Work Method (VWM) [8].
- The Maxwell Stress Tensor (MST) [9].

Previous work on detent force calculation on the studied PMLSM shows that the MST is more adapted to allow a low mesh size in the saturated case with accurate results [10].

A. The Maxwell Stress Tensor

In the case of the Maxwell Stress Tensor (MST), we have to calculate the divergence of the following tensor:

$$T_{ij} = \mu_0 (H_i H_j - \frac{1}{2}\delta_{ij} H^2) \quad with \quad i,j = x,y,z \tag{3}$$

With $\boldsymbol{H}$ the magnetic field given by its values in the Cartesian frame (x,y,z) $\boldsymbol{H}(H_x\ H_y\ H_z)$. δ_{ij} is the Kronecker sign ($\delta_{ij} = 1$ if $i = j$ otherwise $\delta_{ij} = 0$).

The Maxwell Stress Tensor is achieved by a calculation of the force using a surface integration on Γ', over a D' domain. The force can be obtained using the following formula:

$$\mathrm{F} = \int_{\mathrm{D}} \mathrm{div}\mathbf{T}\mathrm{dv} = \oint_{\Gamma'} \mu_0 ((\mathbf{H}.\mathbf{n})\mathbf{H} - \frac{1}{2}|\mathbf{H}|^2\ \mathbf{n})\mathrm{ds} \tag{4}$$

The vector $\boldsymbol{n}$ is normal on the Γ' surface. The Maxwell Stress Tensor presents several advantages, linear or non-linear cases can be evaluated, the choice of the surface integration is undistinguished and only one part of the mesh is concerned.

However, this method is very sensitive to the mesh quality and density in the region where the surface of integration is taken. It is then preferable to have enough air layers on the D' domain surrounding the objects on which the forces have to be calculated. We have noticed that acceptable results were obtainable with at least 4 to 5 air layers [10]. This is particularly the case in the air-gap areas, where there usually are the higher field changes.

The Force calculation is based on the divergence of the Maxwell Stress Tensor [11]. The classical formulation detailed in Eq. 4 also induces that the permeability should be constant and equal to the air permeability. So the force calculation has to be done in the region surrounding the studied object.

B. Meshing consideration

The present study is aimed to highlight the load current effect on the force ripples. Hence, the end-winding effects are neglected. So, according the Figures 2a and 2b, such actuators could be modelled with a 2D-Extruded approach. The FEMM software is then used to compute the force calculation [12].

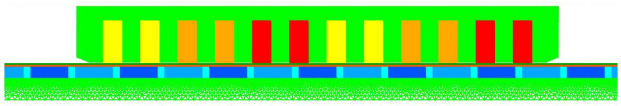

Fig.3. Meshed section of the whole PMLSM [5].

Figure 3 shows that the whole 2D structure of the PMLSM is meshed. Indeed, it is necessary to take into account the end-effect forces. These phenomena are specific to linear motors.

The aim is to obtain some accurate results on the force calculations. So, we have to be particularly careful with the mesh size of each component. Figure 4 shows a zoom on the mesh designed for the actuator (LMD10-050). The added numbers correspond to zones for each material. The rule is to mesh only the zones which are under fast changes of flux density. Zone 4 is called the air eggshell and is composed of two thin meshed layers, which is particularly efficient for the force calculation [10]. Indeed, this air eggshell acts as a cover on the primary ironcore, and allows us to follow more accurately the curve of the flux induced by magnets. The other zones are defined with a larger mesh size than the air-gap, with an auto-adaptation of the mesh to connect with the finer meshed Zone 4 of the air eggshell.

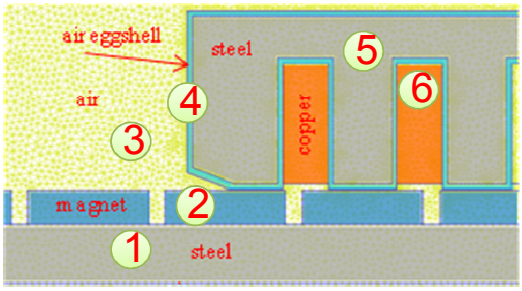

Fig.4. Geometry with mesh size of 0.3 mm [10].

To validate the mesh quality, force calculations are performed at no-load: in Table II, the results at no-load (0A) of the mean force value are sufficiently close to zero with regard to the maximum force ripples from Table I. Indeed, an estimation of the mesh quality can be obtained: the mean value of the detent force is normally null. Nevertheless, the obtained value of 0.15N in the saturated case represents here the accuracy of the results obtained with such a mesh, as in Table II.

C. Calculation principle

Three steps are necessary to calculate the force ripples:

1 – Mesh validation, as previously explained. The aim is to evaluate the calculation error induced by the mesh.

2 – Force calculation using the Maxwell Stress Tensor in a magneto-static analysis in 2D-FEM software [12]. The balanced three-phase currents, with a constant RMS value, are applied according to the position of the PMLSM primary to simulate the self-commutated principle [13]. So, the electromagnetic force is obtained as a function of the current and the magnet position.

3 – For each RMS current value, the mean force is calculated along the position, and then removed from force results to obtain the force ripples.

To be more precise on current generation, the self-commutated principle is explained as followed:

First, the initial position of the mover is chosen to correspond to a first order back-electromotive force (phase to neutral wire) as follows:

$$\begin{cases} emf_{an} = -\hat{e}_a \cdot \sin\left(\pi / \tau_p \cdot x + 0\right) \\ emf_{bn} = -\hat{e}_b \cdot \sin\left(\pi / \tau_p \cdot x + 2\pi/3\right) \\ emf_{cn} = -\hat{e}_c \cdot \sin\left(\pi / \tau_p \cdot x + 4\pi/3\right) \end{cases} \quad (6)$$

Then, in order to generate a constant thrust, the following currents are defined:

$$\begin{cases} i_{a\_ref} = \hat{i} \cdot \sin\left(\pi / \tau_p \cdot x + 0\right) \\ i_{b\_ref} = \hat{i} \cdot \sin\left(\pi / \tau_p \cdot x + 2\pi/3\right) \\ i_{c\_ref} = \hat{i} \cdot \sin\left(\pi / \tau_p \cdot x + 4\pi/3\right) \end{cases} \quad (7)$$

IV. EXPERIMENTAL VALIDATION

The proposed approach is experimentally verified on a laboratory test bench equipped with an ETEL LMD10-050 linear motor and a DS1005 real-time dSPACE Card:

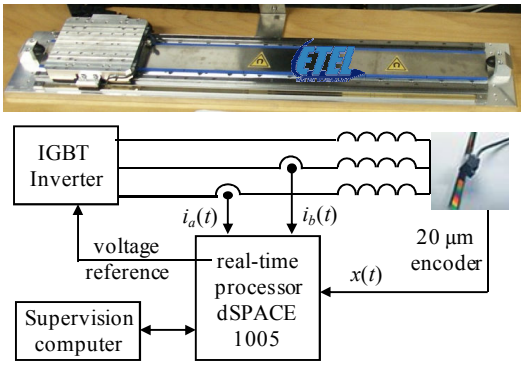

Fig.5. Experimental estimation of the force ripples.

The detent force is estimated using Newton's 2nd law:

$$M \frac{dv}{dt} = T_{em} - T_{ripple} - T_{Coul} - T_{vis} - T_{load} \quad (8)$$

with T_{ripple}, the force ripples, T_{load}, the load force, T_{Coul}, the Coulomb force, $T_{vis} = f_{vis} \cdot v$, the viscous friction force, M, the moving mass, v, the primary velocity and T_{em}, the electromagnetic thrust.

Three steps are necessary to estimate the force ripples:

- First, an identification of the Coulomb and the viscous friction forces is performed at different steady states.
- Then, the electromagnetic force is estimated from the three phase currents, and the magnet position.
- Finally, the force ripples are deduced from Eq. 8. at constant speed.

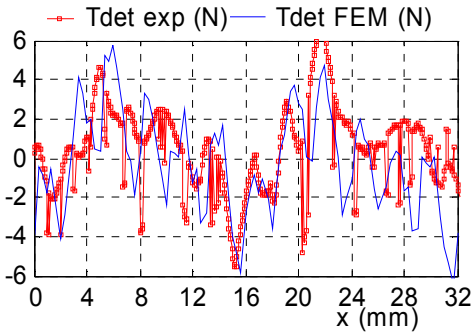

Fig.6. Experimental estimation of the detent force [14].

Figure 6 shows that the FEM and the experimental force ripples are in good accordance. Thus, the proposed approach is experimentally validated. Some fast force peaks can be noticed on the experimental results. They are due to the power electronic commutations of the IGBT inverter.

As an accurate experimental identification (including full range of current values) could be fastidious, further analyses on the current impact on the force ripples will only be presented using the FEM.

V. FEM RESULTS

A. Impact of currents on the force ripples

In the linear case (using a linear characteristic of the ferromagnetic sheets in FEM), the electromagnetic thrust is produced according to the expression of the electromechanical conversion:

$$T_{em} \cdot v = i_a \cdot e_{an} + i_b \cdot e_{bn} + i_c \cdot e_{cn} \qquad (9)$$

with, v the speed; i_a, i_b, i_c, the three phase currents and e_{an}, the back-electromotive force (emf), which is the derivative of the flux Φ_{an} induced by the magnets in phase a. Emf classically has a sinusoidal or trapezoidal waveform depending on the winding distribution. The trapezoidal one is the most common in the industry for linear actuators and gives emf harmonics of rank 3, 5, 7, *etc*. This induces then harmonic force ripples with a frequency equal to 6 times the one of the current. This phenomenon is largely known and well analysed in the literature [15]. Hence, it is possible to subtract it from the rated thrust in order to obtain the other force ripples.

TABLE II
RIPPLE FORCE CALCULATIONS IN THE SATURATED CASE

Current (A_{RMS})	0	5	10	15	20	25
Thrust (N)	0.15	300	568	767	911	1015
Thrust Coefficient Kt (N/A_{RMS})	86.4	85.1	80.5	72.5	64.5	57.5
Max Ripple Force (N)	6	11	26	33	64	97
Ripple force Ratio (%)	-	3,5	4	4,5	7	10

In the saturated case (with Nd-Fe-B permanent magnets of high residual flux density B_r close to 1.2T), the detent forces and the phenomena described above could not be separated anymore, and the finite-element method becomes an effective tool to analyse these ripple forces.

Table II shows that maximum force ripples are about 10% for a 25A current, which makes this phenomenon far from negligible.

Figure 7 presents the results of the electromagnetic force as a function of the RMS current value and the magnet position. Figure 8 shows the results for three currents of 0A, 4A and 8A respectively. Depending on the RMS current level, different phenomena then become preponderant [14]:

- At low current values, the detent force is predominant with force ripples at 12 times the current frequency.
- At high current values, close to the maximal current value, the harmonics of the emf become predominant and induce force ripples at 6 times the current frequency.

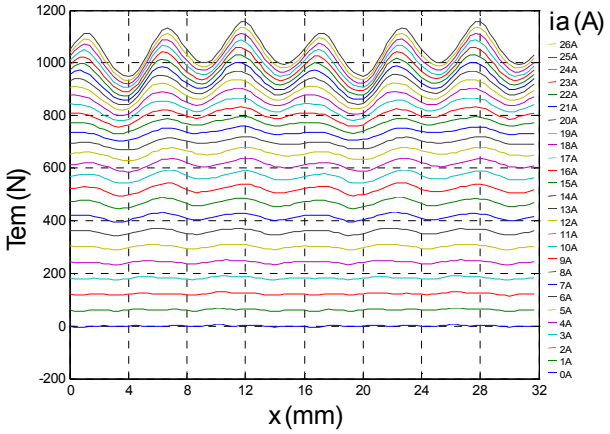

Fig.7. Thrust as a function of currents and magnets position.

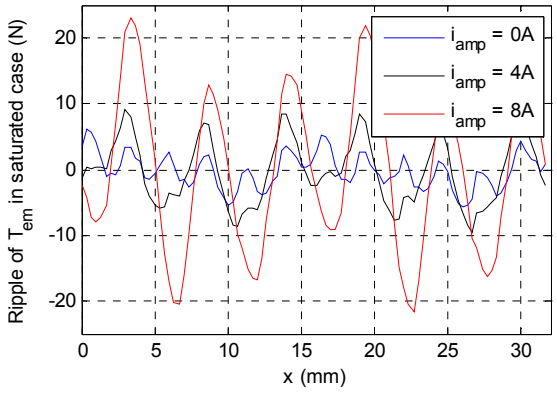

Fig.8. Influence of currents on ripple force of Tem.

B. Impact of currents on the average force

Table II shows that the saturation induces a force decrease of about 33% for a 25A current. Furthermore, we can obtain the electromagnetic thrust waveform as a function of the RMS current value, as in Figure 9.

Table II gives the evolution of Thrust Coefficient K_t, which is the force to the RMS currents ratio. Figure 10 shows the evolution in the linear and in the saturated cases of the K_t parameter. The K_t value from the LMD10-050 datasheet is

88,8N/A_{RMS}, which is close to the FEM results in the linear case presented in Figure 10. This linear K_t parameter is classically used in industrial control design to generate the current references. In the future, this could be improved by using the K_t parameter in the saturated case.

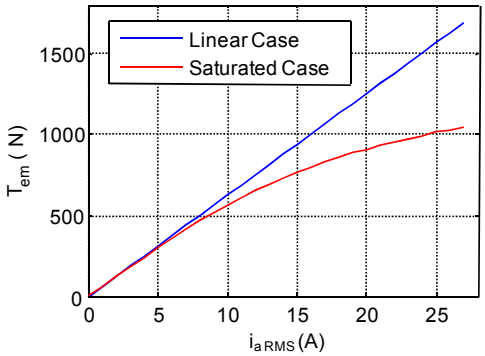

Fig.9. Impact of the saturation on Thrust generation.

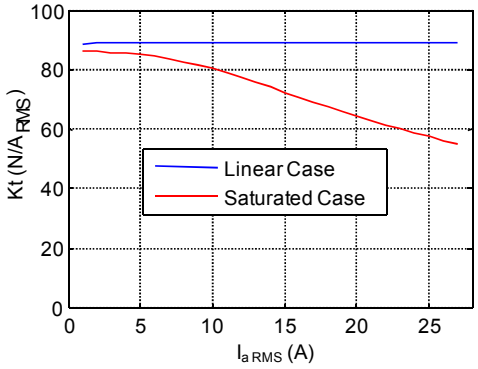

Fig.10. Impact of the saturation on Thrust Coefficient K_t.

VI. CONCLUSION

In this paper, the analyses of the force ripples taking into account the currents supply have been presented for a Flat Ironcore Permanent Magnet Linear Synchronous Motor. The calculation method has been validated thanks to an experimental estimation of the force ripples. Then, the 2D-Finite-Element Method is used because of the large amount of calculation cases. FEM results show that the frequency repartition and the amplitude of the force ripples not only depend on the magnets position, but also on the current amplitude. The force ripples can represent up to 10% of the average thrust.

A variable thrust coefficient K_t is also proposed for industrial force control.

Future work will confirm the presented results using a 3D-FEM that takes into account the end-effects windings. Further investigations on a test bench will be performed to verify the improvement of the control strategy.

ACKNOWLEDGEMENT

This work has been supported by Ralph Coleman of ETEL's Motion Control Research Team, who works actively with the L2EP (Laboratory of Electrical Engineering and Power electronics) of Lille, France.

REFERENCES

[1] A. Cassat, N. Corsi, N. Wavre, and R. Moser, "Direct Linear Drives: Market and Performance Status", *LDIA 2003, Proc. of the 4th Int. Symp. on Linear Drives for Industry Applications*, Birmingham, UK, Sept. 2003.

[2] N. Corsi, R. Coleman, D. Piaget, "Status and new development of linear drives ans subsystems", *LDIA 2007, 6th International Symposium on Linear Drives for Industrial Applications*, Lille, France, ISBN. 978-2-915913-20-0, Sept. 2007.

[3] M.A. Mueller, N.J. Baker, "Modelling the performance of the Vernier hybrid machine", *IEE Proceedings on Electric Power Applications*, Vol. 150, No. 6, pp. 647-654, Nov. 2003.

[4] J. Gomand, G. Remy, A. Tounzi, P.J. Barre, J.P. Hautier, "Impact of Permanent Magnet Field on Inductance Variation of a PMLSM", *EPE 2007, 12th International Conference on Power Electronics and Applications*, Aalborg, Denmark, ISBN: 9789075815108, Sept. 2007.

[5] N. Wavre, "Permanent-Magnet Synchronous Motor", *ETEL patent*, US 05642013A, Jun. 1997.

[6] LMD10-050 Datasheet, *Etel*, http://www.etel.ch, 2007

[7] A. Bossavit, "Force-related Nuts and Bolts in the Discretization Toolkit for Electromagnetics", *COMPUMAG 2007*, Aachen, Germany, pp.885-886, June 2007.

[8] W.N. Fu, P. Zhou, D. Lin, S. Stanton, and Z.J. Cendes, "Magnetic Force Computation in Permanent Magnets Using a Local Energy Coordinate Derivative Method", *IEEE Trans. Magn.*, Vol.40, No.2, Mar. 2004.

[9] F. Henrotte, G. Deliège, K. Hameyer, "The eggshell method for the computation of electromagnetic forces on rigid bodies in 2D and 3D", *CEFC 2002*, Italy.

[10] G. Remy, G. Krebs, A. Tounzi, P.J. Barre, "Finite Element Analysis of a PMLSM (part 1) - Meshing techniques and thrust computations", *LDIA 2007*, 6th International Symposium on Linear Drives for Industrial Applications, Lille, France, Sept. 2007, ISBN: 978-2-915913-20-0

[11] A.N. Wignall, A.J. Gilbert, S.J. Yang, "Calculation of forces on magnetised ferrous cores using the Maxwell stress method", *IEEE Trans. Magn.*, Vol.24, No.1, Jan. 1988.

[12] FEMM, user manual, http://femm.foster-miller.net, 2008.

[13] A.E. Fitzgerald, C. Kingsley, S. Umans, "Electric Machinery", *McGraw-Hill*, 6th Ed., pp.704, ISBN: 0073660094, Jul. 2002.

[14] G. Remy, G. Krebs, A. Tounzi, P.J. Barre, "Finite Element Analysis of a PMLSM (part 2) - Cogging force and end-effect force calculations", *LDIA 2007, 6th International Symposium on Linear Drives for Industrial Applications*, Lille, France, ISBN: 978-2-915913-20-0, Sept. 2007.

[15] J.F. Gieras, Z.J. Piech, "Linear Synchronous Motors, Transportation and Automation Systems", *CRC Press*, ISBN: 0849318599, 1999.